Chapter 13
Measurement of the Mechanical Properties of Biological Tissues

Barry J. Doyle, Ryley A. Macrae and Peter R. Hoskins

Learning outcomes

1. Understand the experimentalconsiderations when mechanically testing ex vivo cardiovascular tissue.
2. Understand the various mechanical test methods used to measure mechanical properties in cardiovascular tissue.
3. Understand imaging based methods for measurement of mechanical properties in cardiovascular tissue.
4. Gain knowledge of the application areas of imaging based methods of estimation of mechanical properties in vivo.

13.1 Introduction

Knowledge of the mechanical behaviour of biological tissue is fundamental to understanding both health and disease, and this is particularly true in the cardiovascular system. For example, arterial tissue stiffens with age and the most conclusive way to measure stiffness is through mechanical testing. This chapter will describe some of the methods used to measure mechanical properties of cardiovascular tissue both in the laboratory and in vivo using medical imaging.

B.J. Doyle (✉) · R.A. Macrae
University of Western Australia, Perth, WA, Australia
e-mail: barry.doyle@uwa.edu.au

P.R. Hoskins
Edinburgh University, Edinburgh, Scotland
e-mail: P.Hoskins@ed.ac.uk

P.R. Hoskins et al. (eds.), *Cardiovascular Biomechanics*,
DOI 10.1007/978-3-319-46407-7_13

13.2 General Considerations for Ex Vivo Methods

13.2.1 Species and Physiology

Animal models have long been used in medical research with the more common models being mouse, rat, rabbit, canine, swine and bovine. There are several considerations needed depending on the animal model, ranging from equipment design to appropriate loading conditions. When performing uniaxial or biaxial testing, the load ranges should conform to those observed in vivo and can be typically inferred from the physiological range of blood pressure and heart rate (e.g. see Table 13.1).

13.2.2 Storage and Tissue Environment

Testing fresh tissue immediately after excision is not always possible. Therefore, storage of the sample is important as tissue degrades (often due to autolysis, which is the self-digestion of or destruction of cells by its own enzymes or microbial activity) over time if not stored in appropriate conditions. Studies have shown that neither refrigeration (Adham et al. 1996) nor freezing (O'Leary et al. 2014a) affect material properties of aortic tissue. However, it is generally recommended that samples be tested within 24 h of excision if possible, otherwise, be immediately frozen. Depending on the tissue type and water content, it may be necessary to use sophisticated techniques to control the rate of freezing to prevent the formation of ice crystals.

Tissue is at approximately 37 °C in vivo and some material properties of arterial tissue change with temperature (Humphrey 2003; Guinea et al. 2005). Heated baths

Table 13.1 Physiological values of human and animal models

Source	Heart rate (Reece 2004)	Pressure	Artery	Axial stretch	
Human	60	120/80 mmHg	Aorta	(1.12–1.30)	Learoyd and Taylor (1966)
			Carotid	1.10	Delfino et al. (1997)
Pig	70–120	150/115 mmHg	Aorta	1.4 (1.2–1.5)	Han and Fung (1995)
		Mésangeau et al. (2000)	Carotid	1.5	Han and Ku (2001)
			Renal	1.232	Rachev and Shazly (2013)
Dog	70–120	140/70 mmHg	Aorta	1.4 (1.2–1.5)	Han and Fung (1995)
		Höglund et al. (2012)	Carotid	1.72	Holzapfel et al. (2000)
Rabbit	180–350	130/65 mmHg (Carli 1974)	Carotid	1.4	Matsumoto et al. (1999)
Mouse	450–750	120/80 mmHg	Aorta	1.4 (1–1.6)	Guo and Kassab (2003)
		Gleason et al. (2004)	Carotid	1.8	Dye et al. (1985)

of physiological solution (e.g. phosphate buffer solution) are used to ensure that material testing is performed at the same temperature as that in vivo.

13.2.3 Preconditioning

Soft tissue exhibits variation (softening) in the loading-unloading curves over the initial series of cycles. This is also observed in filled rubbers and is known as the Mullins effect (Mullins 1969). Preconditioning is performed to overcome this and involves subjecting the sample to a series of loading-unloading cycles until a repeatable curve is obtained. The pre-conditioning protocol should match the desired testing protocol in terms of strain rate so as not to influence the test data. To ensure repeatability, at least 10 cycles should be performed prior to testing.

13.2.4 Tissue Morphology

Microscopy is used to image morphology and structure. After mechanical testing, it is typical to fix the tissue sample in physiological fixative solution (a 4 % buffered solution of formaldehyde), embed in paraffin and sectioned into thin slices (e.g. 5 μm) using a microtome. Many histological stains are available depending on the desired biological component to be imaged; the common stains used in cardiovascular biomechanics being Haematoxylin and Eosin (H&E) to see the cell distribution, or pico-sirius red which stains collagen fibres. There are also specific stains (e.g. Verhoeff-van Gieson's stain that enables the elastin distribution to be visualised). Microscopy can determine changes to the microstructure from different stretch protocols. Furthermore, Scanning Electron Microscopy (SEM) or Transmission Electron Microscopy (TEM) can be used to examine failure regions of the tested sample, such as in the presence of calcified tissue (O'Leary et al. 2015) or during dissection as delamination occurs (Sommer et al. 2008).

13.3 Ex Vivo Measurement of Mechanical Properties

These methods all use samples of excised tissue. The tissues are subject to a known stress causing them to stretch, and the measurement system measures the resulting deformation enabling calculation of strain. From this, the stress-strain behaviour can be determined from which mechanical properties related to elasticity and viscoelasticity can be calculated. In this section a number of methods are described.

13.3.1 Uniaxial Extension

This is the most common mechanical test method and involves controlled stretching of a regular shaped sample in a single direction, often until failure. Dimensions of the sample are precisely measured beforehand particularly in the gauge length (i.e. the length over which data will be extracted). The force and displacement in the direction of elongation is measured throughout the test and used to infer behaviour of the tissue. The techniques used to test cardiovascular tissue have evolved from international industry standards used to test rubber (ASTM International 2013).

Typically, the sample is cut into dumbbell or rectangular shapes, selecting areas of uniform thickness, and mounted in the jaws of the tensile testing system. All dimensions are measured at least three times using either callipers or optical methods (see O'Leary et al. (2013) for the influence of thickness measurement error on data). The samples are mounted to the test machine using flat clamps at both ends of the specimen so as to exert a uniform force over the clamped area. To account for anisotropy (i.e. tissue can behaviour differently in both the circumferential and longitudinal direction), the orientation of the sample's origin is noted. The sample is preconditioned until repeatable mechanical behaviour is observed (e.g. 10 cycles), then elongated until failure. The applied force is measured by the test machine using a load cell. The tissue displacements are measured, either by taking the displacement of the machine head or gauge region markers, or optically via marker tracking (Shazly et al. 2015) or digital image correlation techniques (Zhang et al. 2002; Zhang and Arola 2004). Optical tracking is the preferred option as it measures the true strain of the sample.

The resulting data is a plot of the stress versus the stretch. In mathematical terms, the stretch λ is defined as the fractional change in length of the sample in the unloaded, l_o, and loaded, l, configurations:

$$\lambda = \frac{l}{l_o} \tag{13.1}$$

The stress can be found with reference to the undeformed geometry, known as the first Piola-Kirchoff stress, P, (or often called the 'engineering stress') or with reference to the deformed geometry, known as the Cauchy stress, σ, (often called the 'true stress'). In the case of uniform deformation, these stresses can be found via:

$$P_x = \frac{f_x}{tw} \tag{13.2}$$

$$\sigma_x = \frac{f_x . \lambda_x}{tw} \tag{13.3}$$

where f_x is the applied load, t and w are the reference thickness and width of the specimen in the gauge region, and Eq. 13.3 is derived from the assumed incompressibility of vascular tissue (Chuong and Fung 1984).

The most common parameter describing the mechanical behaviour is the Young' modulus, which is the ratio of stress over strain. This is applicable when the stress-strain behaviour is linear. However, it was noted in Chap. 1 that many biological materials exhibit a non-linear stress-strain relationship. The mechanical behaviour can be characterised by the incremental Young's modulus, which is the slope of the stress/strain curve. More commonly, the stress-strain behaviour is characterised by a non-linear constitutive model containing two or more parameters (the details of such models are beyond the scope of this book; however see Chap. 1 for a brief description).

Uniaxial extension is the most common measurement undertaken to measure mechanical properties related to stiffness. There is measurement of displacement in only one direction (as opposed to two directions in the biaxial system described in the next section); hence, the instrumentation costs are relatively low. For materials, which are anisotropic the stress-strain behaviour will be different depending on the orientation of the material. For example, in arteries the mechanical behaviour is different in the longitudinal and circumferential directions.

13.3.2 Planar Biaxial Extension

This involves stress-strain measurements in a single plane. Simple biaxial testing involves stretching in two directions (x, y) at 90° to each other. More complex systems have the capability of stretching along multiple different directions. Figure 13.1 shows a simple schematic of this test, whereas Fig. 13.2 shows an

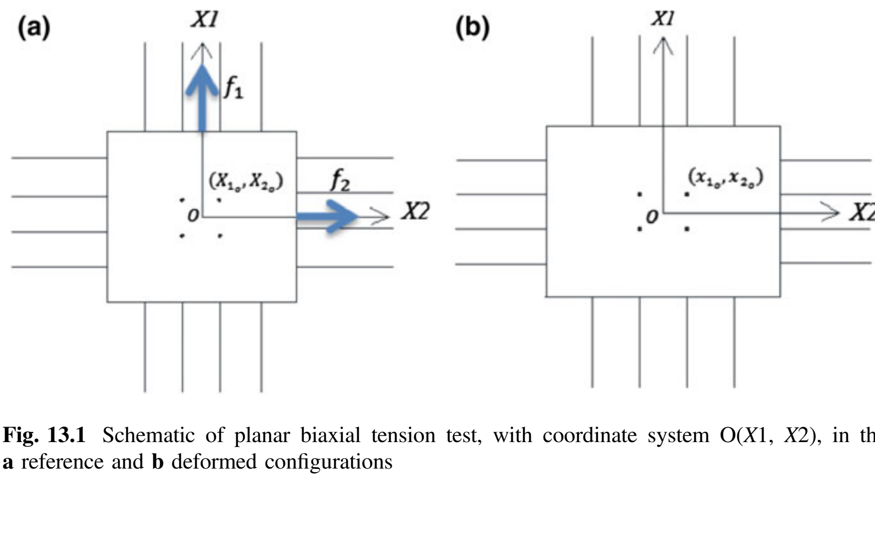

Fig. 13.1 Schematic of planar biaxial tension test, with coordinate system O(X1, X2), in the **a** reference and **b** deformed configurations

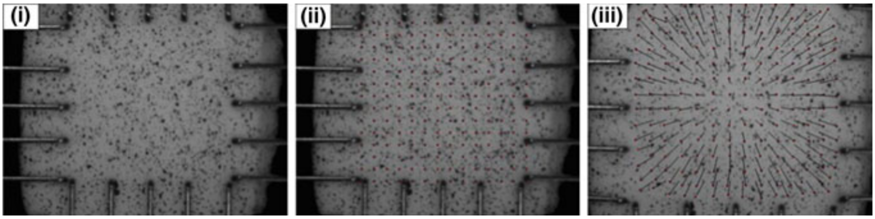

Fig. 13.2 Biaxial testing of intraluminal thrombus. **i** A speckle pattern is applied to the sample surface or **ii** an evenly dispersed grid of virtual points is used by the optical tracking algorithm to produce, **iii** displacement vectors

actual image of a sample of intraluminal thrombus (ILT) under equi-biaxial extension (O'Leary et al. 2013).

Typically, a square specimen is cut from a larger tissue sample. The sample dimensions are measured; sample dimensions are typically much bigger than in uniaxial tests (e.g. 14 × 14 mm in Fig. 13.2). The sample is mounted to the biaxial test machine. Instead of clamps used in uniaxial tests, hooks, barbs and tines are often used. Hooks and barbs can damage the tissue, especially under high strain, and samples can be lost due to failure at the boundaries. Evenly spread tines are the preferred option (as in Fig. 13.2). Loading is applied along each axis and is independently controlled, enabling variable loading rates or different stretch ratios in each direction. The displacement of marks on the central region of the specimen surface is tracked optically (see Fig. 13.2) or by using full-field methods like Electronic Speckle Pattern Interferometry (ESPI) or Digital Image Correlation (DIC). It is important to only examine the central region to avoid the effects present from the attachment area. This is known as Saint-Venant's principle and become negligible beyond a critical distance (decay length) from the grips. For cardiovascular tissue, this central area varies from 16 (Sun et al. 2005) to 25 % (O'Leary et al. 2013, 2014b). The measured positions are expressed in a coordinate system ($x1$, $x2$) and the axial forces are measured using load cells.

The principles for estimation of elastic moduli are similar to that for uniaxial testing in that these are ratios of stress/strain; however, the mathematics is more complex involving tensor equations and hence is provided in the appendix. The reader is referred to Macrae et al. (2016) for more detail.

Biaxial testing is used to obtain data on mechanical properties, which exhibit anisotropy. While planar biaxial testing enables some characterisation of anisotropic behaviour, it does not provide full 3D characterisation; Holzapfel and Ogden (2009) discusses the issue of full 3D characterisation of mechanical properties in detail.

Biaxial testing systems are more expensive that uniaxial testing (in 2016 around £100 k as opposed to £15 k for uniaxial testing), so are less commonly used.

13.3.3 Inflation Testing

Inflation testing is an alternative to tensile testing on excised samples of tissues. The whole vessel is inflated under a controlled pressure and the resulting change in dimensions is measured (Fig. 13.3). This method allows the vessel to maintain the same overall shape as it had in the body, including any pre-stressing, and therefore provides a measurement environment more similar to that in vivo than is possible using tensile testing. The widely cited work on the mechanical properties of whole arteries by Learoyd and Taylor (1966) and Bergel (1961a, b) involved an inflation methodology.

The method involves excising a whole artery and incorporating this into a pressurisation system. Any side branches are tied off to prevent leakage. The artery is stretched to its in vivo length and filled with a fluid such as isotonic saline. Pressure and force measurements are continuously recorded by transducers as the pressure increases/decreases, and the changes in geometry are measured with non-contact methods, such as a Charged Coupled Device (CCD) camera, DIC or by measuring the outer diameter with a precise laser micrometer. The wall thickness can be measured by cutting the vessel into slices after testing or by performing Computed Tomography (CT) imaging on the whole sample prior to testing

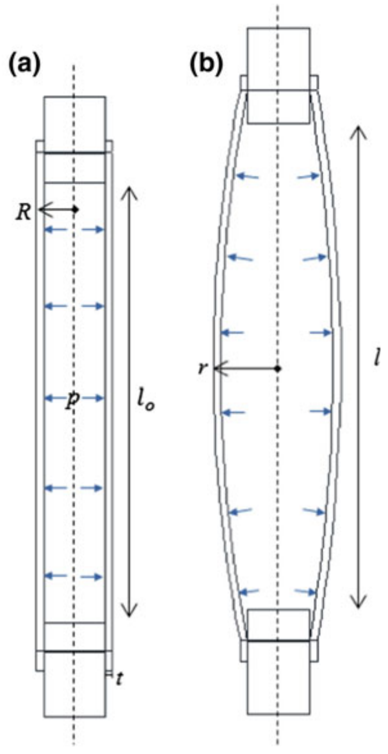

Fig. 13.3 Schematic of inflation-extension test for a cylindrical vessel, in **a** the reference configuration and **b** the deformed configuration

(Doyle et al. 2010). The incremental Young's modulus, E_{inc} can be found from the following equation (from Learoyd and Taylor 1966) which is based on a thin-walled model:

$$E_{\text{inc}} = \frac{P_3 - P_1}{R_{O3} - R_{O1}} \cdot \frac{2(1-\sigma^2)R_{I2}^2 . R_O^2}{(R_{O2}^2 - R_{I2}^2)} \tag{13.4}$$

where σ is the Poisson ratio taken as 0.5; P is the pressure, R_O the outer radius, R_I the inner radius. The subscripts 1, 2, 3 refer to successive measurements at equal pressure differences (e.g. 10 mmHg).

It is important to note that in many cardiovascular applications the sample will be inhomogeneous, thick-walled and anisotropic in behaviour, which leads to significantly more complicated mathematics.

13.3.4 Bioreactor Studies

Bioreactors enable the study of vascular response to transmural pressure, flow rate and axial extension, and often employ inflation-extension tests within a bioreactor chamber. Early experiments involved culturing artery segments in a custom rig, where wall tension was applied via steel wires or by being cultured around a needle (De Mey et al. 1989; Lindqvist et al. 1997) before being subjected to mechanical testing. However, designs have since evolved (McFetridge et al. 2007; Tondreau et al. 2015) and can now accommodate cylindrical specimens (Zaucha et al. 2009) and even much more complicated geometries (e.g. tissue engineered heart valves (Engelmayr et al. 2003)).

13.4 In Vivo Measurement of Mechanical Properties

Measurement of the mechanical properties of tissues may be undertaken in vivo using medical imaging. This section provides some details of work in this area relevant to cardiovascular tissues. Further details on the technology of medical imaging are provided in Chap. 9.

13.4.1 Measurement of Arterial Stiffness from Wall Motion

In Chap. 4 it was described how the elasticity of arteries gives rise to change in diameter through the cardiac cycle associated with the change in blood pressure. Several stiffness indices can be estimated from diameter and pressure changes described in this section. In each case the underlying physical model is that the artery is a uniform homogeneous elastic cylinder.

The Young's modulus E of the arterial wall can be estimated in vivo from these measurements using Eq. 13.5.

$$E = \frac{d_d}{2h} \frac{(P_s - P_d)}{(d_s - d_d)/d_d} \tag{13.5}$$

where h is wall thickness; P_s and P_d are the pressure, and d_s and d_d the diameter, at systole and end-diastole. The elastic modulus is an example of material stiffness.

An index was formulated by Peterson et al. (1960) to provide a stiffness index, which could be used when it was not possible to measure wall thickness. This is called the pressure-strain elastic modulus E_p and is an example of an index of structural stiffness.

$$E_p = \frac{(P_s - P_d)}{(d_s - d_d)/d_d} \tag{13.6}$$

The third index described here is the 'stiffness index' β formulated by Hayashi et al. (1980) to account for the non-linear stress-strain behaviour of arteries. This is also an example of an index of structural stiffness.

$$\beta = \frac{\ln(P_s/P_d)}{(d_s - d_d)/d_d} \tag{13.7}$$

All three quantities above require measurement of the diameter distension and the blood pressure. Typically, an ultrasound system is used to measure diameter distension, an arm cuff is used to measure pressure at systole and diastole and in some arteries (such as the carotid), the ultrasound system can also be used to measure wall thickness. Figure 13.4 shows ultrasound images showing distension and wall thickness measurements.

In abdominal aortic aneurysms, there was no overall difference between E_p in a rupture group and a non-rupture group (Wilson et al. 2003). In patients with atherosclerosis both E and E_p were higher in the contralateral artery in patients with carotid stenosis compared to normal arteries (Claridge et al. 2009). Further reading is provided in Hoskins and Bradbury (2012).

13.4.2 Measurement of Arterial Stiffness from Pulse Wave Velocity

The Moens-Korteweg equation described in Chap. 4 and below (Eq. 13.8) shows that the pulse wave velocity (PWV) is related to Young's modulus E.

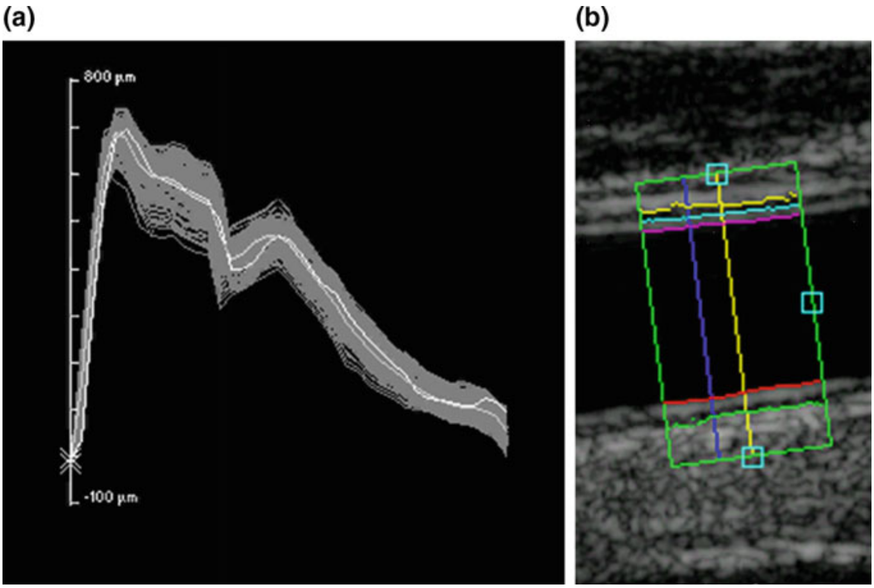

Fig. 13.4 Measurement made using ultrasound for estimation of elastic properties of arteries in vivo; images taken using a Philips HDI 5000 with analysis in HDILab. **a** Diameter-time waveform. **b** Wall thickness (*purple* and *red*—blood/wall interface; *yellow* and *green*—media/adventitia interface)

$$\mathrm{PWV} = \sqrt{\frac{Eh}{d\rho}} \tag{13.8}$$

The Young's modulus may be measured from PWV by rearrangement of the above equation:

$$E = \frac{d\rho}{h}(\mathrm{PWV})^2 \tag{13.9}$$

The PWV may be estimated from the difference in arrival time of the pressure or flow wave at different points in the arterial tree, divided by the distance between points. Commonly the PWV in the aorta is measured from the carotid artery and the femoral artery. These are accessible arteries from which pressure waveforms may be obtained using pressure tonometry or velocity-time flow waveforms obtained using Doppler ultrasound. The distance between the two sites is measured using a tape measure on the patient. When PWV is measured in this manner, it provides a global assessment related to stiffness.

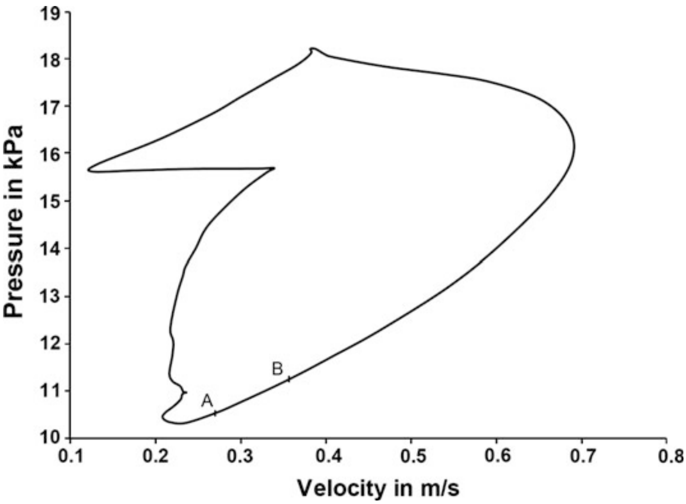

Fig. 13.5 Measurement of local pulse wave velocity from the pressure-velocity loop. Measurement of PWV from a diameter-velocity loop. The start and end points (*A*–*B*) of the linear portions used for the calculation of wave speed. Reprinted from Ultrasound in Medicine and Biology Vol. (35); Rakebrandt et al. (2009), Copyright (2009), with permission from the World Federation for Ultrasound in Medicine and Biology

Local measurement of PWV may be performed by simultaneous measurement of pressure and blood velocity, using the 'water hammer' Eq. (13.10).

$$\frac{dP}{dV} = \rho c \tag{13.10}$$

where P is pressure, V is blood velocity, ρ is blood density and c is PWV.

Early measurements of local PWV were invasive involving flowmeters and pressure transducers positioned on or in the artery (Khir et al. 2001). Non-invasive measurement of local PWV may be performed using tonometry for pressure and Doppler ultrasound for blood velocity (Zambanini et al. 2005), or distension measurement as a surrogate for pressure and Doppler ultrasound for blood velocity (Rabben et al. 2004). The measured velocity and distension produce a loop as shown in Fig. 13.5. The water hammer equation is valid in the region of the curve where there are no reflected waves, so in early systole. The region highlighted shows the curve in early systole from which measurements are made of the slope and from which the PWV may be calculated.

In principle, measurement of PWV could be combined with measurement of wall thickness h and diameter d to estimate local elastic modulus E using Eq. 13.9.

13.4.3 Elastography

Elastography concerns the measurement and imaging of stiffness. In practice, this area is sub-divided into 'strain elastography' and 'shear wave elastography'. A description of the principles of these techniques was given in Chap. 9 where it was noted that strain elastography (as its' name implies) is concerned with the measurement of strain. Strain is used as a surrogate for stiffness on the basis that stiff lesions generally exhibit low strain when a load is applied. True measurement of tissue stiffness in vivo involves the use of shear wave elastography. Briefly shear wave elastography may be undertaken using ultrasound or MRI (where its called 'magnetic resonance elastography' or MRE) and involves the following steps; induction of shear waves in the tissues, use of the imaging system to track the shear waves; measurement of local shear wavelength; estimation of local stiffness E using Eq. 13.11 where c_s is the shear wave velocity and ρ is the local tissue density (the manufacturers assume a value for density).

$$E = 3\rho c_s^2 \tag{13.11}$$

Applications in cardiovascular tissues have mainly concentrated on the heart and used MRI (Kolipaka et al. 2010; Elgeti et al. 2014), see Fig. 13.6. There are a small number of references, which mention shear wave imaging in arteries. Ultrasound shear wave imaging has demonstrated regions of increased stiffness in patients with

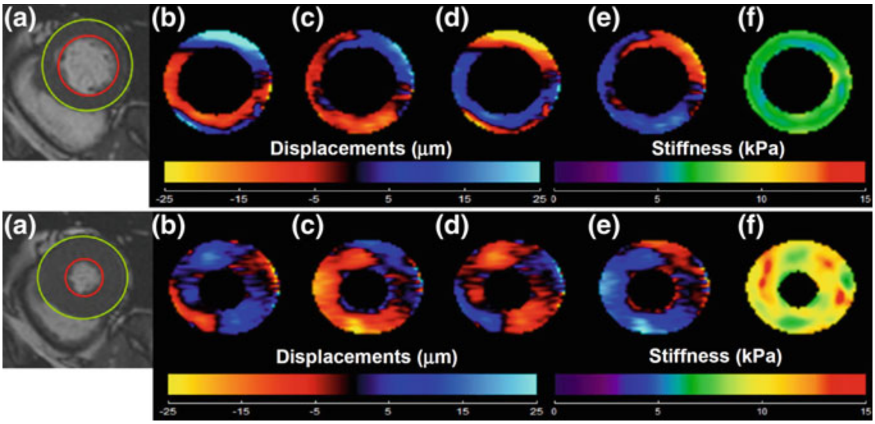

Fig. 13.6 MRE of the heart. *Upper*: images taken at end-diastole. **a** Short-axis magnitude image of the myocardium with epicardial (*green*) and endocardial (*red*) contours. **b–e** The four phases of the through-plane component of the propagating waves. **f** Weighted stiffness map from 3 encoding directions with a mean stiffness of 6.5 ± 0.6 kPa. *Lower*: images taken at end-systole. **a** Short-axis magnitude image of the myocardium. **b–e** The four phases of the through-plane component of the propagating waves and **f** Weighted stiffness map from three encoding directions with a mean stiffness of 9.8 ± 1.5 kPa. Reproduced from Kolipaka et al. (2010); with permission from the International Society for Magnetic Resonance in Medicine (ISMRM), Concord, USA

atherosclerotic plaque (Garrard and Ramnarine 2014; Ramnarine et al. 2014). However, the shear wavelength is long (centimeters) compared to the plaque dimensions (millimetres) so it is unclear whether these measurements are quantitatively correct. Using MRE, images have been produced of the aorta (Woodrum et al. 2006; Kolipaka et al. 2012). However, these are not typical MRE studies in that the propagation of the shear waves in the tissues (in this case the aorta wall) is not measured directly due to spatial resolution limitations. Instead, the shear waves induce a pressure wave in the blood in the aorta. The velocity of this wave is dependent on the thickness and elastic modulus of the aorta, hence stiffness values are actually a composite of these two quantities. At the time of writing, it is unclear whether shear wave elastography is a useful investigative or clinical technique for measurement of cardiovascular tissue stiffness.

References

Adham M, Gournier JP, Favre JP, De La Roche E, Ducerf C, Baulieux J, Barral X, Pouyet M. Mechanical characteristics of fresh and frozen human descending thoracic aorta. J Surg Res. 1996;64:32–4.

ASTM International. ASTM D412–06a. Standard test methods for vulcanized rubber and thermoplastic elastomers—tension. West Conshohocken: ASTM International; 2013.

Bergel DH. The static elastic properties of the arterial wall. J Physiol London. 1961a;156:445–57.

Bergel DH. The dynamic elastic properties of the arterial wall. J Physiol London. 1961b;156:458–69.

Carli G. Blood pressure and heart rate in the rabbit during animal hypnosis. Electroencephalogr Clin Neurophysiol. 1974;37:231–7.

Chuong CJ, Fung YC. Compressibility and constitutive equation of arterial wall in radial compression experiments. J Biomech. 1984;17:35–40.

Claridge MW, Bate GR, Hoskins PR, Adam DJ, Bradbury AW, Wilmink AB. Measurement of arterial stiffness in patients with peripheral arterial disease: are changes in vessel wall more sensitive than intima-media thickness? Atherosclerosis. 2009;205:477–80.

De Mey JG, Uitendaal MP, Boonen HC, Vrijdag MJ, Daemen MJ, Struyker-Boudier HA. Acute and long-term effects of tissue culture on contractile reactivity in renal arteries of the rat. Circ Res. 1989;65:1125–35.

Delfino A, Stergiopulos N, Moore JE Jr, Meister JJ. Residual strain effects on the stress field in a thick wall finite element model of the human carotid bifurcation. J Biomech. 1997;30:777–86.

Doyle BJ, Cloonan AJ, Walsh MT, Vorp DA, McGloughlin TM. Identification of rupture locations in patient-specific abdominal aortic aneurysms using experimental and computational techniques. J Biomech. 2010;43:1408–16.

Dye WW, Gleason RL, Wilson E, Humphrey JD. Altered biomechanical properties of carotid arteries in two mouse models of muscular dystrophy. J Appl Physiol. 1985;2007(103):664–72.

Elgeti T, Knebel F, Hättasch R, Hamm B, Braun J, Sack I. Shear-wave amplitudes measured with cardiac MR elastography for diagnosis of diastolic dysfunction. Radiology. 2014;271:681–7.

Engelmayr GC Jr, Hildebrand DK, Sutherland FW, Mayer JE Jr, Sacks MS. A novel bioreactor for the dynamic flexural stimulation of tissue engineered heart valve biomaterials. Biomaterials. 2003;24:2523–32.

Garrard JW, Ramnarine KV. Shear-wave elastography in carotid plaques: comparison with grayscale median and histological assessment in an interesting case. Ultraschall Med. 2014;35:1–3.

Gleason RL, Gray SP, Wilson E, Humphrey JD. A multiaxial computer-controlled organ culture and biomechanical device for mouse carotid arteries. J Biomech Eng. 2004;126:787–95.

Guinea GV, Atienza JM, Elices M, Aragoncillo P, Hayashi K. Thermo-mechanical behaviour of human carotid arteries in the passive state. Am J Physiol Heart Circulatory Physiol. 2005. doi:10.1152/ajpheart.01099.2004.

Guo X, Kassab GS. Variation of mechanical properties along the length of the aorta in C57bl/6 mice. Am J Physiol Heart Circ Physiol. 2003;285:H2614–22.

Han HC, Fung YC. Longitudinal strain of canine and porcine aortas. J Biomech. 1995;28:637–41.

Han HC, Ku DN. Contractile responses in arteries subjected to hypertensive pressure in seven-day organ culture. Ann Biomed Eng. 2001;29:467–75.

Hayashi K, Handa H, Nagasawa S, Okumura A, Moritake K. Stiffness and elastic behavior of human intra-cranial and extra-cranial arteries. J Biomech. 1980;13:175–85.

Höglund K, Hanås S, Carnabuci C, Ljungvall I, Tidholm A, Häggström J. Blood pressure, heart rate, and urinary catecholamines in healthy dogs subjected to different clinical settings. J Vet Intern Med. 2012;26:1300–8.

Holzapfel GA, Ogden RW. On planar biaxial tests for anisotropic nonlinearly elastic solids. A continuum mechanical framework. Math Mech Solids. 2009;14:474–89.

Holzapfel GA, Gasser T, Ogden R. A new constitutive framework for arterial wall mechanics and a comparative study of material models. J Elast Phys Sci Solids. 2000;61:1–48.

Hoskins PR, Bradbury AW. Wall motion analysis. In: Nicolaides A, Beach KW, Kyriakou E, Pattichis CS, editors. Ultrasound and carotid bifurcation atherosclerosis. Springer, 2012. pp. 325–339.

Humphrey JD. Continuum thermomechanics and the clinical treatment of disease and injury. Appl Mech Rev. 2003;56:231–60.

Khir AW, O'Brien A, Gibbs JSR, Parker KH. Determination of wave speed and wave separation in the arteries. J Biomech. 2001;34:1145–55.

Kolipaka A, Araoz PA, McGee KP, Manduca A, Ehman RL. In vivo cardiac MR elastography in a single breath hold. Proc Int Soc Magn Reson Med. 2010;18:591.

Kolipaka A, Woodrum D, Araoz PA, Ehman RL. MR elastography of the in vivo abdominal aorta: a feasibility study for comparing aortic stiffness between hypertensives and normotensives. J Magn Reson Imaging. 2012;35:582–6.

Learoyd BM, Taylor MG. Alterations with age in viscoelastic properties of human arterial walls. Circ Res. 1966;18:278–92.

Lindqvist A, Nilsson BO, Hellstrand P. Inhibition of calcium entry preserves contractility of arterial smooth muscle in culture. J Vasc Res. 1997;34:103–8.

Macrae RA, Miller K, Doyle BJ. Methods in mechanical testing of arterial tissue: a review. Strain. 2016;52:380–99.

Matsumoto T, Okumura E, Miura Y, Sato M. Mechanical and dimensional adaptation of rabbit carotid artery cultured in vitro. Med Biol Eng Comput. 1999;37:252–6.

McFetridge PS, Abe K, Horrocks M, Chaudhuri JB. Vascular tissue engineering: bioreactor design considerations for extended culture of primary human vascular smooth muscle cells. ASAIO J. 2007;53:623–30.

Mésangeau D, Laude D, Elghozi JL. Early detection of cardiovascular autonomic neuropathy in diabetic pigs using blood pressure and heart rate variability. Cardiovasc Res. 2000;45:889–99.

Mullins L. Softening of rubber by deformation. Rubber Chem Technol. 1969;42:339–62.

O'Leary SA, Doyle BJ, McGloughlin TM. Comparison of methods used to measure the thickness of soft tissues and their influence on the evaluation of tensile stress. J Biomech. 2013;46:1955–60.

O'Leary SA, Doyle BJ, McGloughlin TM. The impact of long term freezing on the mechanical properties of porcine aortic tissue. J Mech Behav Biomed Mater. 2014a;37:165–73.

O'Leary SA, Healey DA, Kavanagh EG, Walsh MT, McGloughlin TM, Doyle BJ. The biaxial biomechanical behavior of abdominal aortic aneurysm tissue. Ann Biomed Eng. 2014b;42:2440–50.

O'Leary SA, Mulvihill JJ, Barrett HE, Kavanagh EG, Walsh MT, McGloughlin TM, Doyle BJ. Determining the influence of calcification on the failure properties of abdominal aortic aneurysm (AAA) tissue. J Mech Behav Biomed Mater. 2015;42:154–67.

Peterson LH, Jensen RE, Parnell J. Mechanical properties of arteries in vivo. Circ Res. 1960;8:622–39.

Rabben SI, Stergiopulos N, Hellevik LR, Smiseth OA, Slørdahl S, Urheim S, Angelsen B. An ultrasound-based method for determining pulse wave velocity in superficial arteries. J Biomech. 2004;37:1615–22.

Rachev A, Shazly T. A preliminary analysis of the data from an in vitro inflation-extension test can validate the assumption of arterial tissue elasticity. J Biomech Eng. 2013;135:84502. doi:10.1115/1.4024665.

Rakebrandt F, Palombo C, Swampillai J, Schon F, Donald A, Kozakova M, Kato K, Fraser AG. Arterial wave intensity and ventricular-arterial coupling by vascular ultrasound: rationale and methods for the automated analysis of forwards and backwards running waves. Ultrasound Med Biol. 2009;35:266–77.

Ramnarine KV, Garrard JW, Kanber B, Nduwayo S, Hartshorne TC, Robinson TG. Shear wave elastography imaging of carotid plaques: feasible, reproducible and of clinical potential. Cardiovasc Ultrasound. 2014;12:49.

Reece WO (ed). Duke's physiology of domestic animals, 12th ed. Sage House, 512 East State Street, Ithaca, New York 14850, Cornell University Press. 2004.

Shazly T, Rachev A, Lessner S, Argraves W, Ferdous J, Zhou B, Moreira AM, Sutton M. On the uniaxial ring test of tissue engineered constructs. Exp Mech. 2015;55:41–51.

Sommer G, Gasser TC, Regitnig P, Auer M, Holzapfel GA. Dissection properties of the human aortic media: an experimental study. J Biomech Eng. 2008;130:021007. doi:10.1115/1.2898733.

Sun W, Sacks MS, Scott MJ. Effects of boundary conditions on the estimation of the planar biaxial mechanical properties of soft tissues. J Biomech Eng. 2005;127:709–15.

Tondreau MY, Laterreur V, Gauvin R, Vallières K, Bourget JM, Lacroix D, Tremblay C, Germain L, Ruel J, Auger FA. Mechanical properties of endothelialized fibroblast-derived vascular scaffolds stimulated in a bioreactor. Acta Biomater. 2015;18:176–85.

Wilson KA, Lee AJ, Lee AJ, Hoskins PR, Fowkes FG, Ruckley CV, Bradbury AW. The relationship between aortic wall distensibility and rupture of infrarenal abdominal aortic aneurysms. J Vasc Surg. 2003;37:112–7.

Woodrum DA, Romano AJ, Lerman A, Pandya UH, Brosh D, Rossman PJ, Lerman LO, Ehman RL. Vascular wall elasticity measurement by magnetic resonance imaging. Magn Reson Med. 2006;56:593–600.

Zambanini A, Cunningham SL, Parker KH, Khir AW. McG Thom SA, Hughes AD. Wave-energy patterns in carotid, brachial, and radial arteries: a noninvasive approach using wave-intensity analysis. Am J Physiol Heart Circulatory Physiol. 2005;289:H270–6.

Zaucha MT, Raykin J, Wan W, Gauvin R, Auger FA, Germain L, Michaels TE, Gleason RL Jr. A novel cylindrical biaxial computer-controlled bioreactor and biomechanical testing device for vascular tissue engineering. Tissue Eng Part A. 2009;15:3331–40.

Zhang D, Arola DD. Applications of digital image correlation to biological tissues. J Biomed Opt. 2004;9:691–9.

Zhang D, Eggleton C, Arola D. Evaluating the mechanical behavior of arterial tissue using digital image correlation. Exp Mech. 2002;42:409–16.